Journal of Materials Chemistry C

Accepted Manuscript

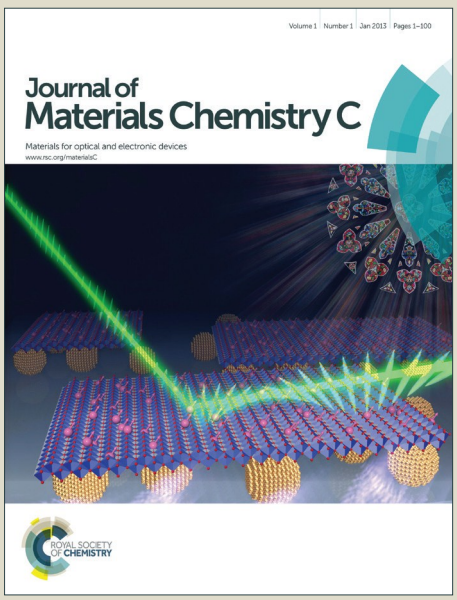

ROYAL SOCIETY OF CHEMISTRY

www.rsc.org/materialsC

Graphical Abstract

The core-shell ternary ZnS/Ni_3S_2@Ni composite exhibits superior electromagnetic wave absorption properties, which were attributed to synergistic effect between dielectric loss and magnetic loss, multiple interfacial polarization, good impedance match and unique urchin-like structure.

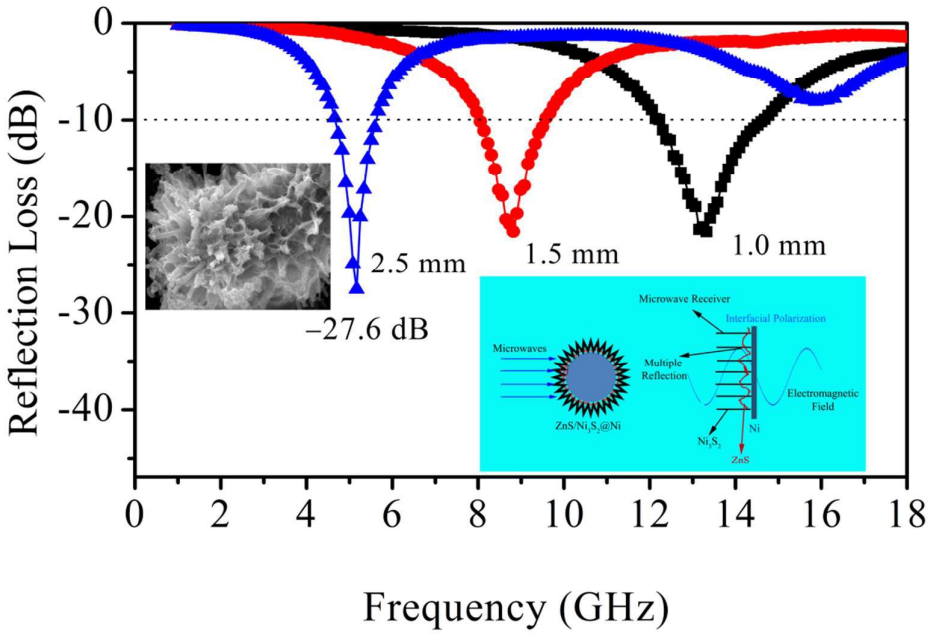

In-situ synthesis of novel urchin-like ZnS/Ni_3S_2@Ni composite with core-shell structure as an efficient electromagnetic absorption absorber

Biao Zhao [a], Gang Shao [a] *, Bingbing Fan [a], Wanyu Zhao [a], Shihao Zhang [a], Keke Guan [a], Rui Zhang [a, b] *

Received (in XXX, XXX) Xth XXXXXXXXX 20XX, Accepted Xth XXXXXXXXX 20XX
DOI: 10.1039/c000000x

ABSTRACT: The novel urchin-like ZnS/Ni_3S_2@Ni composite with core-shell structure was successfully synthesized by a facile two-stage method. The structure and morphology are investigated by X-ray diffraction, scanning electron microscopy, transmission electron microscopy and energy dispersive spectrometry. The influence of reaction temperatures on the structure and morphology of ZnS/Ni_3S_2@Ni products were investigated by the aid of XRD and SEM techniques. A plausible formation mechanism of core-shell urchin-like architectures was proposed based on temperature dependent experiments. The electromagnetic absorption measurements show that the urchin-like ZnS/Ni_3S_2@Ni composite possesses the outstanding electromagnetic absorption properties compared with other ZnS/Ni_3S_2@Ni composites. The optimal reflection loss of –27.6 dB can be observed at 5.2 GHz and the effective absorption (below -10 dB, 90% electromagnetic absorption) bandwidth is 2.5 GHz (12.2-14.7 GHz) with the thin thickness of 1.0 mm. The location of minimal reflection loss can be tuned between 4.6 GHz and 18.0 GHz for the absorber with the thin thickness in 0.8−2.5 mm. The enhanced electromagnetic absorption properties were attributed to synergistic effect between dielectric loss and magnetic loss, multiple interfacial polarization resulting from the heterogeneous structures of core-shell ternary ZnS/Ni_3S_2@Ni composite, good impedance match and unique urchin-like structure.

1. Introduction

The explosive development of information technology using electromagnetic waves in both civil and military fields leads to great concerns on electromagnetic interference (EMI) issues, which is expected to consider a new type of challenge on information security and physical health nowadays.[1, 2] Therefore, considerable attention has been devoted to exploring effective electromagnetic absorbing materials with broad bandwidth and highly efficient absorption properties. Electromagnetic absorbers, which is distinct from the conventional reflection principles in electromagnetic shielding, provide an alternative to eliminate the unwanted electromagnetic (EM) waves by converting the EM energy into thermal energy or dissipating the EM waves through interference.[3, 4]

In recent years, great efforts have been done to exploit the composite with core-shell structure, which is suit for the electromagnetic absorption absorber. [5, 6] Ohlan et al. prepared core-shell structured poly (3,4-Ethylenedioxy Thiophene)-barium ferrite nanocomposites and the minimal reflection loss is -22.5 dB at 15 GHz. [7] Zhou et al. synthesized core-shell Fe_3O_4-poly(3, 4-ethylenedioxythiophene) microspheres and the minimum reflection loss reached approximated -30 dB with the thickness of 4 mm. Moreover, the electromagnetic absorption properties of the composites are significantly influenced by the (EDOT)/(Fe_3O_4) ratio.[8] Core–shell composites, Fe_3O_4@C, with 500 nm Fe_3O_4 microspheres as cores were prepared by Du and co-workers. The thickness of carbon shell, from 20 to 70 nm, can be well controlled. In comparison with pure Fe_3O_4, coating Fe_3O_4 microspheres with carbon shells endowed the composites with enhanced electromagnetic absorption properties due to multiple relaxation processes in these core-shell heterogeneous system.[9] Core–shell structured Fe_3O_4–polyaniline nanoparticles were synthesized by Sun et al. Compared with pristine Fe_3O_4, the core-shell structured composites show enhanced electromagnetic absorption with the optimal reflection loss of -35.1 dB observed at 16.7 GHz. The excellent electromagnetic properties are ascribed to the dielectric resonance arising from the special magnetic nanoparticle–conducting polymer core–shell structure.[10] Yang et al [11] designed Silica coated mesoporous Fe (Fe@SiO_2) microcubes with high performance electromagnetic wave attenuation in comparison with Fe cubes. In our previous literatures, the Ni based core-shell composites, such as Ni@SnO_2,[12] Ni/CuO,[13] and Ni@Al_2O_3 [14] exhibit the enhanced

electromagnetic wave absorption properties compared with raw Ni microspheres.

From above reported results, the electromagnetic wave absorption properties of core-shell composites are superior to these of individual materials. In these composites, magnetic materials act as cores and dielectric materials regard as shells, which can provide cooperative effect between dielectric loss and magnetic loss, thus enhancing electromagnetic absorption capabilities. Moreover, these core-shell composites are mainly bimaterials. There are scarce reports about electromagnetic wave absorption properties of ternary core-shell composites.[15, 16]

Nanomaterial properties are dependent on the size, shape, and dimensionality. Metal sulfide nanomaterials have attracted significant attention because of their excellent properties and promising applications in electronic and optoelectronic devices. Nickel subsulfide and ZnS are of importance in the metal sulfide family [17,18] because of the their variety applications such as in lithium ion batteries, supercapacitors, dye-sensitized [19, 20] and charge transfer, anion exchange, electricity generation,[21,22] respectively. Due to the semiconductor properties of nickel subsulfide and ZnS, it can induce dipole and space charge polarizations when placed under the alternated electromagnetic field.[23, 24] Moreover, nickel subsulfide (Ni_3S_2) are highly metallic compared to insulating oxide compounds, which can cause conductive loss when irradiated by electromagnetic waves.[25] The core-shell Ni@ZnS composites with the improvement of electromagnetic properties were reported by our earlier literatures.[26, 27] However, to the best of our knowledge, the electromagnetic wave absorption core-shell structured ternary ZnS/Ni_3S_2@Ni composite was hardly found in the published papers. In this work, a novel ZnS/Ni_3S_2@Ni composite with core-shell structure was successfully synthesized. The urchin-like core-shell ZnS/Ni_3S_2@Ni composite obtained at 120 ºC exhibits the excellent electromagnetic absorption and the absorption mechanism of such unique hierarchical microstructure was also discussed in detail.

2. Experimental section

All the reagents are commercial available without any further purification. $N_2H_4{\cdot}H_2O$ (80%), $ZnCl_2$, and trisodium citrate were bought from Guangfu Chemical Co. Ltd. (Tianjin, China). Nickel chloride hexahydrate ($NiCl_2{\cdot}6H_2O$), sodium hydroxide (NaOH), 1,2-isopropanol and sodium acetate were purchased from Xilong Chemical Reagent Co. Ltd. (Guangdong, China). $Na_2S{\cdot}9H_2O$ was provided by Kemiou Chemical Reagent Co. Ltd. (Tianjin, China) and Fengchuan Chemical Reagent Technologies Co. Ltd. (Tianjin, China), respectively. The preparation process of urchin-like ZnS/Ni_3S_2@Ni core-shell structured composites containing two steps: synthesis of Ni microspheres and subsequent growth of ZnS/Ni_3S_2 on the surfaces of Ni microspheres.

2.2 Preparation of monodispersed Ni microspheres

The monodipersed Ni microspheres were prepared according to our previous literatures.[13, 14, 27] Simply, $NiCl_2{\cdot}6H_2O$ (1.2 g), trisodium citrate (0.3 g) and sodium acetate (3.0 g) were dissolved in the 60mL 1,2-isopropanol. Subsequently, $N_2H_4{\cdot}H_2O$ (6 mL) was added into above mixture before transferred into Teflon-lined autoclave. The sealed autoclave was heated at 140 ºC for 15 h in an oven. The final products was washed with anhydrous ethanol and distilled water several times, and vacuum-dried at 60 ºC for 12 h.

2.3 Synthesis of urchin-like core-shell structured ZnS/Ni_3S_2@Ni composite

In brief, Ni (0.05 g) was dispersed in a mixture of aqueous solution of distilled water (30 mL) and ethanol (30 mL) containing 1.0 M NaOH. Then, 1 mmol $ZnCl_2$ and 2 mmol $Na_2S{\cdot}9H_2O$ were introduced into above mixture, respectively. The mixed solution was transferred to a Teflon-lined autoclave. The sealed autoclave was heated to 120 ºC for 15 h. The products were washed in turn with distilled water and anhydrous ethanol, and then dried at 60 ºC overnight in vacuum. To probe the possible formation mechanism of urchin-like core-shell structure and effects of temperatures on the morphologies of final products, the temperature-dependent experiments (60 ºC, 80 ºC , 100 ºC and 120 ºC) were also carried out in this work.

2.4 Characterization

The composition and phase purity of the as-received sample were analysed by an X-ray diffraction (XRD, XD-3, Beijing Purkinje General Instrument Co. Ltd.). The microscopic morphology and microstructure of the samples were observed using transmission electron microscope (TEM, JEOL JSM-2100) and field-emission scanning electron microscope (FESEM, JSM-7001F) associated with an energy dispersive X-ray spectroscopy (EDS, Oxford Instruments). The electromagnetic parameters were measured on a vector network analyzer (Agilent, N5224A) in the range of 1–18 GHz band at room temperature. The composite samples for electromagnetic parameters measurements were prepared by evenly mixing the product with a paraffin wax in mass ratio of 1:1, and then being pressed into a ring with an outer diameter of 7.0 mm, inner diameter of 3.0 mm. Herein, the paraffin serves as binder, which is transparent to electromagnetic wave.

3. Results and discussion

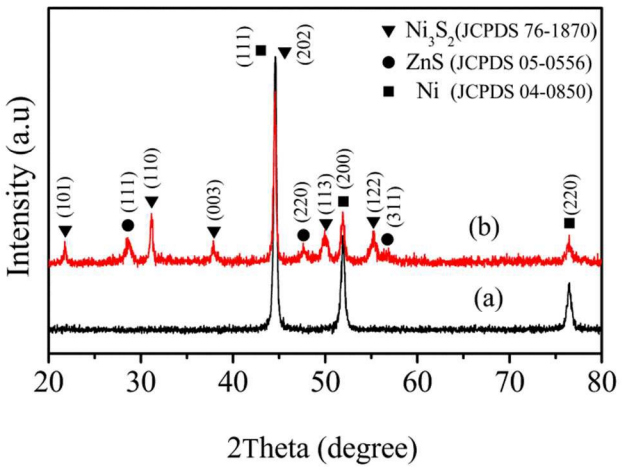

Figure 1 XRD patterns of (a) pristine Ni microspheres and (b) as-prepared ZnS/Ni_3S_2@Ni.

The phase composition and structure of the as-prepared Ni microspheres and urchin-like ZnS/Ni_3S_2@Ni products were examined by XRD. Fig.1a shows the XRD pattern of pristine Ni microspheres, which can be well indexed to face-centred cubic structure of Ni (JCPDS No. 040850). As shown in Fig.1b, besides the diffraction peaks of Ni, the other diffraction peaks can be readily assigned to the zinc-blende ZnS (JCPDS Card no. 05-0566) and Ni_3S_2 (JCPDS Card no 76-1870). From these XRD patterns, it can be confirmed that the core-shell ZnS/Ni_3S_2@Ni composite consists of nickel, nickel sulfide and zinc sulfide. It can be inferred that nickel has functioned as the template for formation of Ni_3S_2 and deposition of ZnS.

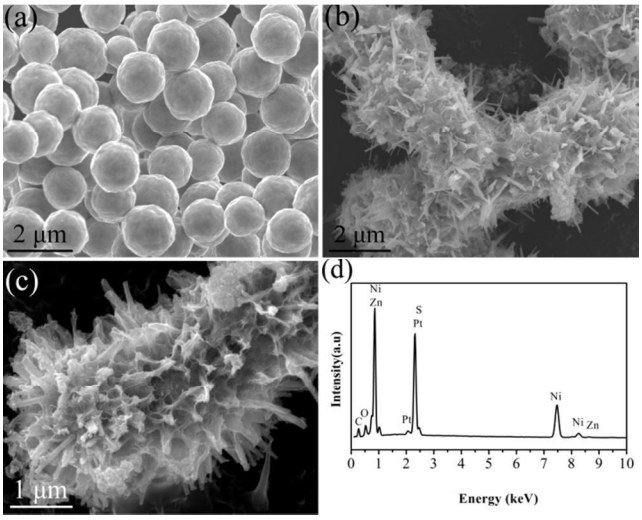

Figure 2 FESEM images of (a) Ni microspheres, (b-c) urchin-like core-shell structured ZnS/Ni_3S_2@Ni composite; (d) EDS profile of ZnS/Ni_3S_2@Ni composite.

To investigate the morphology of the products, FESEM images are taken for Ni microspheres and ZnS/Ni_3S_2@Ni composite and the corresponding results were shown in Fig.2. From the Fig.2a, it can be seen that Ni products were composed of uniform distribution and smooth surface of microspheres with the average diameter of about 1 μm. Fig.2(b,c) show the different magnification FESEM images of core-shell ZnS/Ni_3S_2@Ni composite. Interestingly, from panoramic observation (Fig.2b), urchin-like products were optionally grown on the surfaces of Ni microspheres and the outline of Ni spheres cannot be clearly observed due to the formation of ZnS/Ni_3S_2 on the surface of Ni particles. Notably, the diameter of Ni particles was also decreased, which indicates the consumption of Ni products. The length and diameter of thorns were about 1 μm and 50 nm, respectively. Close observation from the high magnification FESEM image (Fig.2c), the presence of crinkled products

encircle Ni particles and the crinkled products are expected to be links between Ni particles and thorns. Fig. 2d presents the EDS spectra of the ZnS/Ni_3S_2@Ni composite. The EDS spectrum reveals the presence of elements of S, Zn and Ni. Pt peaks are also seen in the EDS curve because the SEM sample was prepared by sputtering of platinum onto the sample. Moreover, the high magnification FESEM images and corresponding elemental mapping were shown in Fig. S1. From the Fig.S1(a,b), it is noteworthy that the ZnS/Ni_3S_2@Ni composites possess the features of urchin-like structure structure. The element mappings of Ni, Zn, and S are presented in Fig.S1(c−e), respectively. Interestingly, element Zn shows the larger area in the rim region than that in the center, which indicates that the ZnS/ Ni_3S_2 urchins were grown on Ni particles to form core-shell structure.

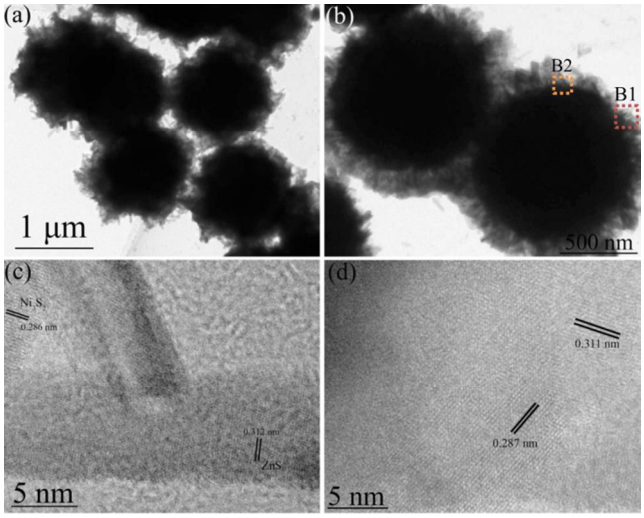

Figure 3 (a,b) TEM image of core-shell structured ZnS/Ni_3S_2@Ni composite; (c) HRTEM image recorded on the B1 area in the Fig.3b, (d) HRTEM image recorded on the B2 area in the Fig.3b.

Detailed structural information about the ZnS/Ni_3S_2@Ni composite was further analysed by TEM and HRTEM. As exhibited in Fig. 3 (a,b), the TEM image of the ZnS/Ni_3S_2@Ni composite shows that Ni microspheres have a coarse outer layer and core-shell structure of composite can be clearly observed due to different contrast of cores and shells. Notably, the crinkled products and thorn-like products are both grown on the surfaces of Ni microspheres, which is in accordance with the observation of above FESEM images (Fig.2b,c). Fig. 3 (c,d) shows a high-resolution TEM (HRTEM) image recorded from the rim regions of core-shell composite, respectively (as seen in Fig. 3b). From the Fig.3c, the HRTEM image derived from the B1 area in the Fig.3b indicates that the spacing of the lattice is 0.286 nm and 0.312 nm, which correspond to the spacing of (110) and (111) planes of Ni_3S_2 and ZnS, respectively. Based on these results, it can be confirmed that the shell products are comprised of Ni_3S_2 and ZnS materials. Furthermore, the HRTEM image recorded from the B2 region in Fig.3b was shown in Fig.3d. The lattice fringe spacing of 0.287 nm and 0.311 nm were in accordance with Ni_3S_2 and ZnS, respectively. Notably, it can be found the Ni_3S_2 phase was located in the place which is close to the core of Ni spheres. Thus, the composite is ZnS/Ni_3S_2@Ni. The Ni_3S_2 stays away from the core of Ni spheres.

To study the influences of reaction temperature on the microstructure of final products, the temperature dependent experiments were carried out and the corresponding results were presented in Fig.(4,5). Fig.4 shows the XRD patterns of ZnS/Ni_3S_2@Ni composites prepared at various temperatures. All the diffraction peaks can be well attributed to the Ni, ZnS and Ni_3S_2 phases. No additional other peaks can be observed in the profiles, indicating the core-shell structured composites prepared at different temperatures were the mixture phases of ZnS, Ni_3S_2 and Ni. Interestingly, the relative intensity of Ni_3S_2 diffraction peaks was increased with increasing the reaction temperatures while the relative intensity of ZnS diffraction peaks clearly reduces, which indicates that the high crystallinity Ni_3S_2 products are supposed to generate at relatively high temperatures (120 ºC)

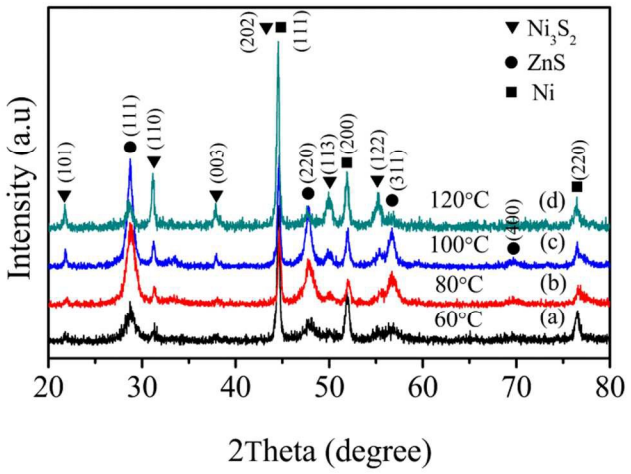

Figure 4 XRD curves of ZnS/Ni_3S_2@Ni composites prepared at different reaction temperatures: (a) 60 °C, (b) 80 °C, (c) 100 °C and 120 °C.

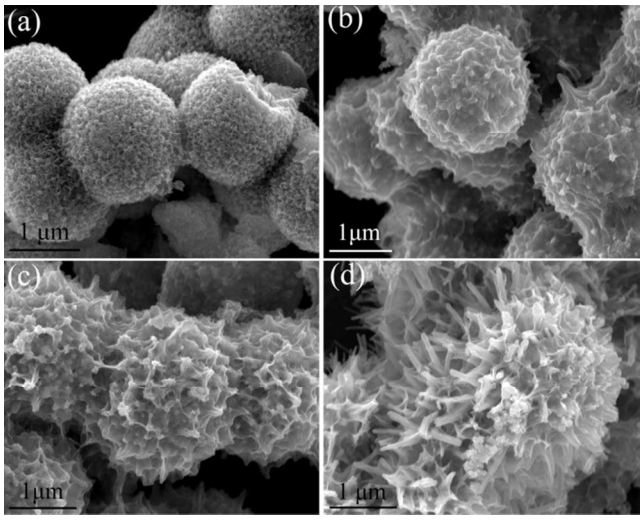

Figure 5 FESEM images of core-shell ZnS/Ni_3S_2@Ni composites prepared at various reaction temperatures: (a) 60 °C, (b) 80 °C, (c) 100 °C and (d) 120 °C.

It is assumed that the reaction temperature has an effect on the morphology of core-shell heterstructure. At low temperature (60 ºC), interestingly, there are plentiful waxberry-like products existed in Fig.5a. It is due to the fact that Ni microspheres were coated by wrinkle ZnS products. Meanwhile, combination of XRD patterns (Fig.4), Ni_3S_2 nanoparticles were in-situ formed by consumption of Ni particles and then deposited on the surface of remaining Ni products. With increasing the reaction temperatures to high temperatures (80 ºC), notably, some protuberant prickles were grown the surfaces of core-shell composites (Fig.5b). When the reaction temperature is 100 ºC, more and strong protuberant prickles existed on the wrinkle surfaces of composite can be clearly observed (Fig.5c). With further increasing the temperature to 120 ºC, the target urchin-like core-shell structured ZnS/Ni_3S_2@Ni composites were produced with a large number of thorns or rods grown on the rugged surfaces.

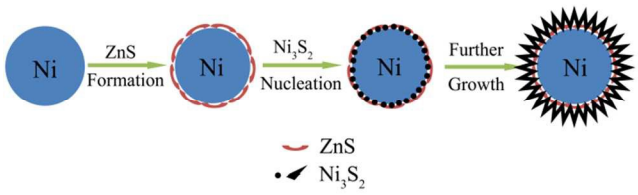

Figure 6 A plausible formation mechanism of urchin-like core-shell structured ZnS/Ni_3S_2@Ni composites

Based on the temperature dependent experiments, a possible plausible formation mechanism of urchin-like core-shell structured ZnS/Ni_3S_2@Ni composites was proposed (Fig.6). Firstly, when $ZnCl_2$ and $Na_2S·9H_2O$ were introduced into this reaction process, it is not hard to understand that ZnS nanoparticles were yielded immediately generated from the reaction between $ZnCl_2$ and Na_2S due to the high solubility-product constant (Ksp) of ZnS (Ksp $=2.93\times10^{-25}$).[21,22] According to our earlier reports,[26] the ZnS products are prone to form wrinkle and rough samples. Therefore, the Ni microspheres were coated by wrinkle ZnS at early stage. Secondly, because of high concentration of Na_2S (2 mmol), the unreacted Na_2S would be reacted with Ni microspheres to produce Ni_3S_2 products. [17] Thirdly, the fresh Ni_3S_2 are expected to grow to thorns or rods.[19] Thus, the urchin-like core-shell structured ZnS/Ni_3S_2@Ni composites were formed.

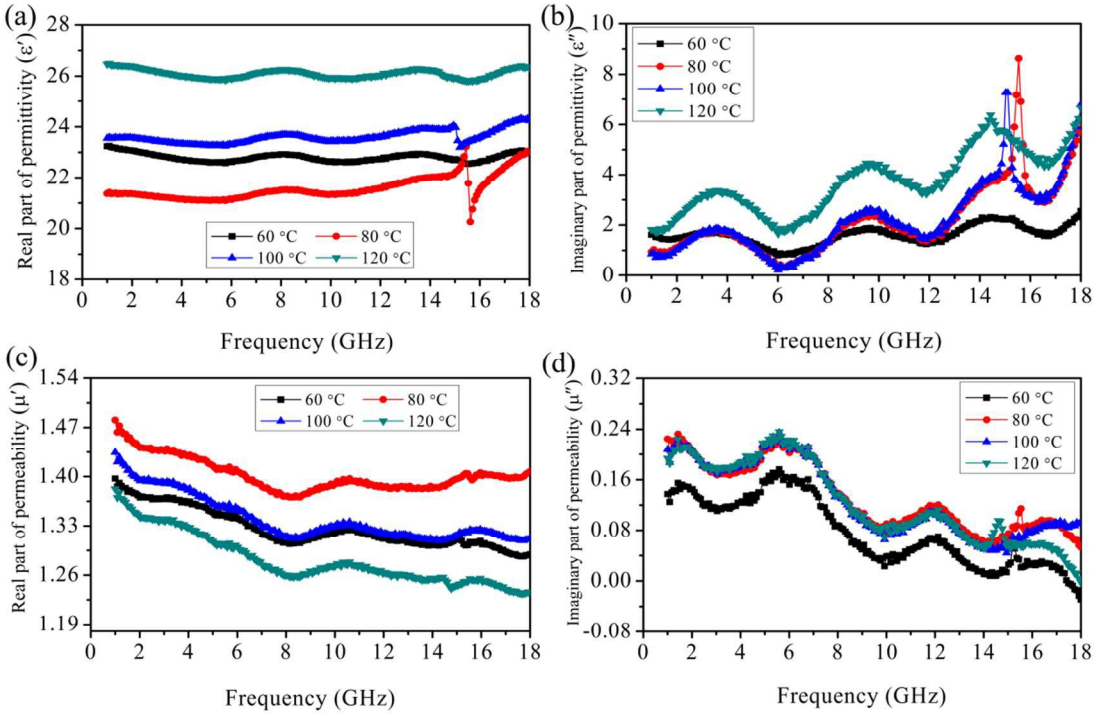

Figure 7 Frequency dependence of (a) real parts (ε′) and (b) imaginary parts (ε″) of ZnS/Ni_3S_2@Ni composites prepared at various temperatures; (c) real parts (μ′) and (b) imaginary parts (μ″) of ZnS/Ni_3S_2@Ni composites prepared at various temperatures.

Fig. 7 (a,b) exhibit the frequency dependencies of the real (ε′) and imaginary parts (ε″) of relative complex permittivity of the ZnS/Ni_3S_2@Ni composites prepared at different temperatures. It is well known that the ε′ is vitally correlated with the amount of polarization happening in the material, and ε″ is associated to energy dissipation. [8, 28] The performance of relative permittivity was related with ionic, electronic, orientational, and space-charge polarization (interfacial polarization).[14, 29] It can be observed that the real parts (ε′) of ZnS/Ni_3S_2@Ni paraffin composites almost show the steady values with little fluctuation (Fig.7a). Notably, the ε′ values of ZnS/Ni_3S_2@Ni composites prepared at 80 ℃ and 100 ℃ show the sharp peaks located at about 15-16 GHz. It may be due to the formation of unique fresh thorns, which can regard as links between Ni microspheres and wrinkle ZnS to form conductive gateway, leading to relatively high conductive. [30, 31] Fig.7b presents the imaginary parts (ε″) of four core-shell ZnS/Ni_3S_2@Ni composites. Notably, it can be seen that urchin-like ZnS/Ni_3S_2@Ni composite shows the highest ε″ values among the four samples cover almost measured frequency, which indicates the highest dielectric loss for the urchin-like ZnS/Ni_3S_2@Ni sample. Interestingly, the four ZnS/Ni_3S_2@Ni samples present the similar increase trend and multi-peaks on the ε″ values, meaning multiple resonances behavior. This resonance behavior is generally associated with highly conductive and electronic spin, skin effects,[32] space charge polarizations, and polarized centers.[25] These phenomena are also clearly observed in our earlier literatures. [13, 26, 27] The observed increase in ε″ with increasing frequency was assigned to the augment in interfacial polarization. [33] In a heterogeneous system, the accumulation of space charges at the interface of two materials will result in interfacial polarization and is known as Maxwell–Wagner polarization. [34, 35] Herein, plentiful heterogeneous interfaces in urchin-like core-shell ZnS/Ni_3S_2@Ni composite make contribution to interfacial polarization. According to the free electron theory, [36] $\varepsilon'' \approx 1/\pi\varepsilon_0\rho f$, where ρ is the resistivity, high ε″ indicates high conductivity. As shown in Fig.8b, urchin-like core-shell ZnS/Ni_3S_2@Ni composite exhibit high conductivity at the nearly whole frequency. Notably, ZnS/Ni_3S_2@Ni composites prepared at 80 ℃ and 100 ℃ show the relatively high conductivity at about 15-16 GHz, which is accordance with above

discussion of real parts (ε′). For the urchin-like core-shell ZnS/Ni_3S_2@Ni sample, the wrinkle ZnS and similar metal Ni_3S_2 thorns on the surfaces of Ni spheres can connect with each other and a continuous microcurrent gradually produces, which will cause low electric resistivity and induce electric and conduction loss.

The real part (μ′) and the imaginary part (μ″) of complex permeability of the ZnS/Ni_3S_2@Ni composites as a function of frequency from 1 to 18 GHz are shown in Fig. 7(c,d). The μ′ values show a decrease trend in the 1–18 GHz frequency range (Fig.7c). Moreover, from the Fig.7d, μ″ values present three broad peaks in the measured frequency. These multi-resonance peaks of μ″ can be attributed to the natural resonance at low frequency and 'exchange mode' resonance at high frequency, [37, 38] which may be associated with the small size effect and shape anisotropy. In general, the contribution to magnetic loss contains domain-wall displacement, magnetic hysteresis, eddy current and natural resonance.[23] Herein, the magnetic loss was mainly attributed to natural resonance loss due to the weak applied electromagnetic field.[39] It is expected that the natural resonance will result in strong magnetic loss abilities in low frequency, while the interfacial polarization takes place in high frequency. This complementary effect is helpful for enhancement of electromagnetic absorption properties.

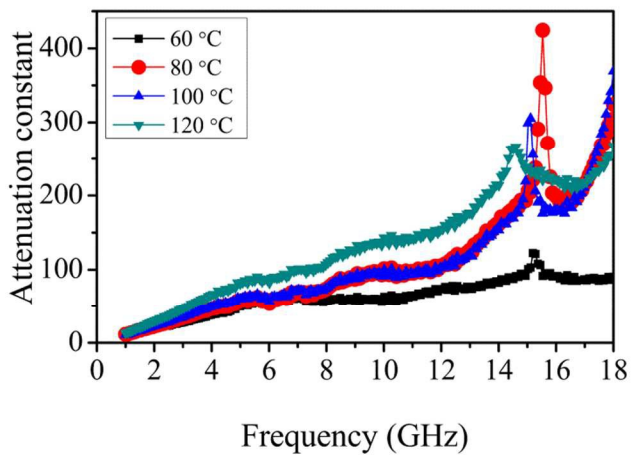

Figure 8 Attenuation constant of four core-shell ZnS/Ni_3S_2@Ni paraffin-composites versus frequency

Nevertheless, it is difficult to judge the electromagnetic absorption properties just relying on the electromagnetic parameters (impedance match), which let the electromagnetic wave go through the interior of absorber as much as possible. In fact, if we want to obtain the enhanced electromagnetic absorption properties, another important factor should also be considered, namely electromagnetic wave attenuation (α). The attenuation constant α which determines the attenuation properties of absorbing materials, which can be expressed by following equation [6, 40]

$$\alpha = \frac{\sqrt{2}\pi f}{c} \times \sqrt{(\mu''\varepsilon'' - \mu'\varepsilon') + \sqrt{(\mu''\varepsilon'' - \mu'\varepsilon')^2 + (\mu'\varepsilon'' + \mu''\varepsilon')^2}} \quad (1)$$

In which f and c are the frequency and velocity of light, respectively. Fig. 8 exhibits the dependence of the attenuation constant α of ZnS/Ni_3S_2@Ni paraffin-composites in the frequency range of 1–18 GHz. It can be noteworthy that the urchin-like ZnS/Ni_3S_2@Ni prepared at 120 °C shows the largest attenuation constant in the almost whole measured frequency range, which indicates its excellent electromagnetic absorption.

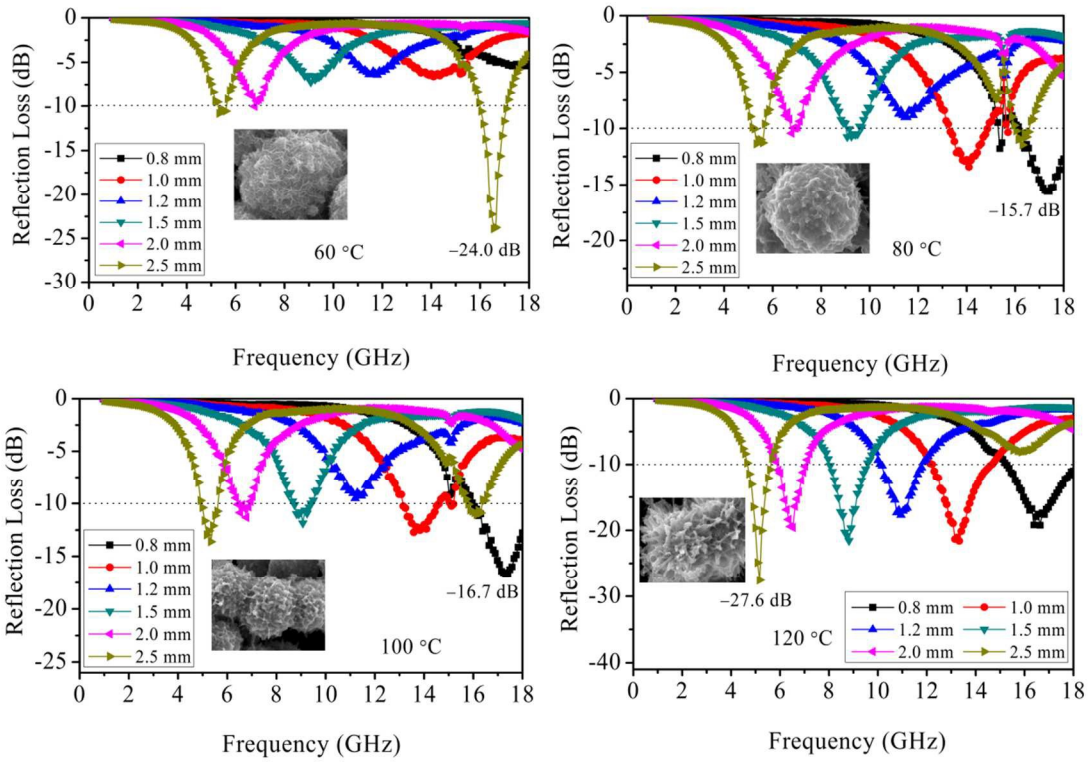

Figure 9 The calculated reflection loss of core-shell ZnS/Ni_3S_2@Ni composites prepared at various temperatures: (a) 60 °C, (b) 80 °C, (c) 100 °C and (d) 120 °C with different thickness in the frequency range of 1-18 GHz.

To reveal the electromagnetic wave absorption properties, the representation reflection loss (RL, which can be used to judge the electromagnetic absorption abilities of absorber, the lower the value, the stronger the absorption) of the core-shell ZnS/Ni_3S_2@Ni paraffin-composites with different sample thicknesses are simulated based on the measured complex permeability ($\mu_r = \mu' - j\mu''$) and complex permittivity ($\varepsilon_r = \varepsilon' - j\varepsilon''$) according to the transmit line theory, which can be described as the following equations: [11, 41, 42]

$$RL = 20\log_{10}\left|(Z_{in} - Z_0)/(Z_{in} + Z_0)\right| \quad (2)$$

$$Z_{in} = Z_0\sqrt{\frac{\mu_r}{\varepsilon_r}}\tanh\left(j\frac{2\pi fd\sqrt{\mu_r\varepsilon_r}}{c}\right) \quad (3)$$

In which Z_{in} is the input characteristic impedance, Z_0 is the impedance of free space, f is the frequency, c is the velocity of light, and d is the absorber thickness. Fig.9 shows the reflection loss (RL) of the core-shell ZnS/Ni_3S_2@Ni composites prepared at different temperatures with thickness varies from 0.8 to 2.5 mm in the frequency range of 1-18 GHz. It can be found that urchin-like ZnS/Ni_3S_2@Ni composite exhibits outstanding electromagnetic absorption. The minimal RL is down to -27.6 dB at 5.2 GHz as the thickness is 2.5 mm. Notably, the reflection loss of urchin-like ZnS/Ni_3S_2@Ni can reach -21.6 dB at 13.3 GHz when the absorber thickness is only 1.0 mm, and the effective bandwidth (RL less than -10 dB) is 2.5 GHz (12.2-14.7 GHz), which is superior to those of other reported dielectric/magnetic composites, such as Fe@SnO_2(-10.1dB),[43] and Co/CoO(-14 dB).[44] In fact, most of similar absorbing materials [13, 27, 43-49] are hardly obtain outstanding microwave absorption at the identical 1.0 mm, as listed in the Table 1. At the same time, the attenuation peaks would shift to lower frequencies and two RL peaks could be observed with the increasing thickness bigger than 2.5 mm. It can be attributed to the quarter-wavelength cancellation model. [50]

Table 1 The reflection loss data of some similar samples.

Sample	Minimum RL value (dB)	thickness (mm)	Frequency range (RL<-10 dB) (GHz)	Ref.

Ni/SnO_2	-18.6	7.0	13.8–15.3	[13]
PS@PPy@Ni	–20.06	2.0	9.16–13.75	[45]
Ni/Polypyrrole	–15.2	2.0	11–15.4	[46]
Ni/ZnS	–20.06	2.7	11.52–16.24	[27]
Fe/SnO_2	>-10	1.5	None	[43]
Co/CoO	–14.5	2.5	12.24–15.68	[44]
Fe/graphene	-15	1.5	16.0-18.0	[47]
α-Fe_2O_3@$CoFe_2O_4$	-15.2	1.5	14.8-18.0	[48]
MnO_2@Fe–graphene	–17.5	1.5	14-18	[49]
ZnS/Ni_3S_2@Ni	–21.6	1.0	12.2-14.7	present work

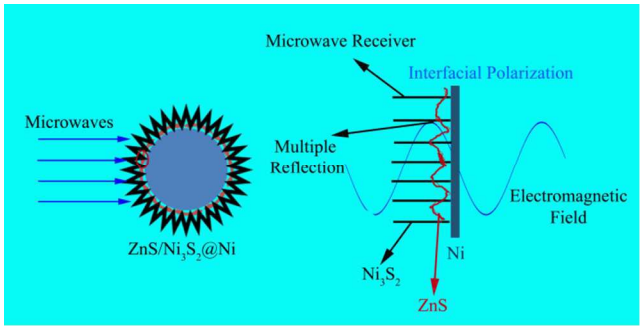

Figure 10 Schematic illustration of plausible electromagnetic wave absorption mechanism for the core-shell ZnS/Ni_3S_2@Ni heterogeneous system.

Based on above analysis, a plausible electromagnetic wave absorption mechanism for the core-shell ZnS/Ni_3S_2@Ni heterogeneous system was proposed, as depicted in Fig.10. When the ZnS/Ni_3S_2@Ni composite is subjected to electromagnetic wave radiation, the Ni_3S_2 thorns grown on the surfaces of Ni microspheres are expected as antenna receiver to allow electromagnetic waves penetrate into interior of absorber as much as possible, namely called good impedance match. [33, 51] Moreover, electromagnetic absorption is also understood from the viewpoint of Ohmic heating induced by an alternating magnetic field, [52] in which ZnS/Ni_3S_2@Ni composite with relatively high electric conductivity from high ε″ values. Thirdly, Due to the heterogeneous systems of core-shell ZnS/Ni_3S_2@Ni composites, the multi-interfaces between the ZnS, Ni_3S_2, and Ni are beneficial for enhancement of electromagnetic wave absorption because of the interaction of electromagnetic radiation with charged multipoles at the interfaces. [53, 54] The interfacial polarization [34, 55] happening at the interfaces is attributed to the migration of charge carriers through different dielectric properties of the composite material, which gives rise to charge accumulation at the interfaces. During the activation of an electromagnetic wave, an additional interfacial relaxation is generated, which is helpful for the electromagnetic absorption.[56] Finally, the synergistic effect between dielectric loss at high frequency and magnetic loss at low frequency also makes contribution to the improvement of electromagnetic absorption. [57]

4. Conclusion

In summary, novel and interesting urchin-like ZnS/Ni_3S_2@Ni composites were synthesized through a two-step process including solution reduction and subsequent template method. The morphologies of core-shell ZnS/Ni_3S_2@Ni composites were crucially determined by the reaction temperatures. Based on serials of contrast experiments, a possible formation mechanism of urchin-like core-shell ZnS/Ni_3S_2@Ni composite was proposed. Different ZnS/Ni_3S_2@Ni composites prepared at different temperatures show variable electromagnetc absorption responses, in which the urchin-like ZnS/Ni_3S_2@Ni obtained at 120 ºC displays the best electromagnetic absorption performance due to its promising dielectric loss and magnetic loss, improved matched characteristic impedance, as well as unique urchin-like structure. Multiple dielectric resonances originating from effective accumulation of various polarizations in the urchin-like structure are considered to be responsible for the enhancement of electromagnetic absorption. It is believed that the in-situ synthesis of core-shell ZnS/Ni_3S_2@Ni composites may open up a new avenue for the design and preparation of novel microwave absorbers with promising application potential.

Acknowledgements

The authors appreciate the financial support from the National Natural Science Foundation of China (Grant No. 51172213)

Notes and references

[a] *School of Materials Science and Engineering, Zhengzhou University, Zhengzhou 450001, China*

[b] *Laboratory of Aeronautical Composites, Zhengzhou Institute of Aeronautical Industry Management, Zhengzhou 450046, China*

** Corresponding Author.*

Dr. Gang Shao

E-mail address: gang_shao@zzu.edu.cn

Prof. Rui Zhang

Tel: +86-371-60632007

Fax: +86-371-60632600

E-mail address: zhangray@zzu.edu.cn

1. L. Tian, X. Yan, J. Xu, P. Wallenmeyer, J. Murowchick, L. Liu and X. Chen, *J. Mater. Chem. A*, 2015, 3, 12550-12556.
2. Y. Zhang, Y. Huang, T. Zhang, H. Chang, P. Xiao, H. Chen, Z. Huang and Y. Chen, *Adv. Mater.*, 2015, 27, 2049-2053.
3. G. Wang, Z. Gao, S. Tang, C. Chen, F. Duan, S. Zhao, S. Lin, Y. Feng, L. Zhou and Y. Qin, *ACS Nano*, 2012, 6, 11009-11017.
4. Y.-H. Chen, Z.-H. Huang, M.-M. Lu, W.-Q. Cao, J. Yuan, D.-Q. Zhang and M.-S. Cao, *J. Mater. Chem. A*, 2015, 3, 12621-12625.
5. Y.-J. Chen, G. Xiao, T.-S. Wang, Q.-Y. Ouyang, L.-H. Qi, Y. Ma, P. Gao, C.-L. Zhu, M.-S. Cao and H.-B. Jin, *J. Phys. Chem. C*, 2011, 115, 13603-13608.
6. G. Wang, X. Peng, L. Yu, G. Wan, S. Lin and Y. Qin, *J. Mater. Chem. A*, 2015, 3, 2734-2740.
7. A. Ohlan, K. Singh, A. Chandra and S. K. Dhawan, *ACS Appl. Mater. Interfaces*, 2010, 2, 927-933.
8. W. Zhou, X. Hu, X. Bai, S. Zhou, C. Sun, J. Yan and P. Chen, *ACS Appl. Mater. Interfaces*, 2011, 3, 3839-3845.
9. Y. Du, W. Liu, R. Qiang, Y. Wang, X. Han, J. Ma and P. Xu, *ACS Appl. Mater. Interfaces*, 2014, 6, 12997-13006.
10. Y. Sun, F. Xiao, X. Liu, C. Feng and C. Jin, *RSC Adv.*, 2013, 3, 22554-22559.
11. Z. Yang, Z. Li, L. Yu, Y. Yang and Z. Xu, *J. Mater. Chem. C*, 2014, 2, 7583-7588.
12. B. Zhao, G. Shao, B. Fan, W. Li, X. Pian and R. Zhang, *Mater. Lett.*, 2014, 121, 118-121.
13. B. Zhao, G. Shao, B. Fan, W. Zhao and R. Zhang, *Phys. Chem. Chem. Phys.*, 2015, 17, 6044-6052.
14. B. Zhao, G. Shao, B. Fan, W. Zhao and R. Zhang, *RSC Adv.*, 2014, 4, 57424-57429.
15. B. Shen, W. Zhai, M. Tao, J. Ling and W. Zheng, *ACS Appl. Mater. Interfaces*, 2013, 5, 11383-11391.
16. Y. Li, D. Chen, X. Liu, Y. Zhou, Q. Zhuang, R. Cai and K. Zhang, *Compos. Sci. Technol.*, 2014, 100, 212-219.
17. C. W. Lee, S.-D. Seo, H. K. Park, S. Park, H. J. Song, D.-W. Kim and K. S. Hong, *Nanoscale*, 2015, 7, 2790-2796.
18. X. Huang, M.-G. Willinger, H. Fan, Z.-l. Xie, L. Wang, A. Klein-Hoffmann, F. Girgsdies, C.-S. Lee and X.-M. Meng, *Nanoscale*, 2014, 6, 8787-8795.
19. Y. Liao, K. Pan, Q. Pan, G. Wang, W. Zhou and H. Fu, *Nanoscale*, 2015, 7, 1623-1626.
20. Z. Wang, X. Li, Y. Yang, Y. Cui, H. Pan, Z. Wang, B. Chen and G. Qian, *J. Mater. Chem. A*, 2014, 2, 7912-7916.
21. W. Xitao, L. Rong and W. Kang, *J. Mater. Chem. A*, 2014, 2, 8304-8313.
22. Y.-P. Zhu, J. Li, T.-Y. Ma, Y.-P. Liu, G. Du and Z.-Y. Yuan, *J. Mater. Chem. A*, 2014, 2, 1093-1101.
23. H. Wang, H. Guo, Y. Dai, D. Geng, Z. Han, D. Li, T. Yang, S. Ma, W. Liu and Z. Zhang, *Appl. Phys. Lett.*, 2012, 101, 083116.
24. Q. Zhang, C. Li, Y. Chen, Z. Han, H. Wang, Z. Wang, D. Geng, W. Liu and Z. Zhang, *Appl. Phys. Lett.*, 2010, 97, 133115.
25. P. C. P. Watts, W. K. Hsu, A. Barnes and B. Chambers, *Adv. Mater.*, 2003, 15, 600-603.
26. B. Zhao, G. Shao, B. Fan, W. Zhao, Y. Chen and R. Zhang, *RSC Adv.*, 2015, 5, 9806-9814.

27. B. Zhao, G. Shao, B. Fan, W. Zhao, Y. Xie and R. Zhang, *RSC Adv.*, 2014, 4, 61219-61225.
28. L. Wang, X. Jia, Y. Li, F. Yang, L. Zhang, L. Liu, X. Ren and H. Yang, *J. Mater. Chem. A*, 2014, 2, 14940-14946.
29. L. Jiang, Z. Wang, D. Li, D. Geng, Y. Wang, J. An, J. He, W. Liu and Z. Zhang, *RSC Adv.*, 2015, 5, 40384-40392.
30. L. Wang, Y. Huang, X. Sun, H. Huang, P. Liu, M. Zong and Y. Wang, *Nanoscale*, 2014, 6, 3157-3164.
31. G. Tong, F. Liu, W. Wu, F. Du and J. Guan, *J. Mater. Chem. A*, 2014, 2, 7373-7382.
32. H. Li, Y. Huang, G. Sun, X. Yan, Y. Yang, J. Wang and Y. Zhang, *J. Phys. Chem. C*, 2010, 114, 10088-10091.
33. G. Tong, J. Yuan, W. Wu, Q. Hu, H. Qian, L. Li and J. Shen, *CrystEngComm*, 2012, 14, 2071-2079.
34. Q. Liu, D. Zhang and T. Fan, *Appl. Phys. Lett.*, 2008, 93, 013110.
35. H. Wu, H. Li, G. Sun, S. Ma and X. Yang, *J. Mater. Chem. C*, 2015, 3, 5457-5466.
36. X. Liu, D. Geng, H. Meng, P. Shang and Z. Zhang, *Appl. Phys. Lett.*, 2008, 92, 173117.
37. T. Liu, P. Zhou, J. Xie and L. Deng, *J. Appl. Phys.*, 2012, 111, 093905.
38. P. Toneguzzo, O. Acher, G. Viau, F. Fiévet-Vincent and F. Fievet, *J. Appl. Phys.*, 1997, 81, 5546-5548.
39. X. F. Zhang, X. L. Dong, H. Huang, Y. Y. Liu, W. N. Wang, X. G. Zhu, B. Lv, J. P. Lei and C. G. Lee, *Appl. Phys. Lett.*, 2006, 89, 053115.
40. J. Xiang, J. Li, X. Zhang, Q. Ye, J. Xu and X. Shen, *J. Mater. Chem. A*, 2014, 2, 16905-16914.
41. G. Pan, J. Zhu, S. Ma, G. Sun and X. Yang, *ACS Appl. Mater. Interfaces*, 2013, 5, 12716-12724.
42. X. Chen, F. Meng, Z. Zhou, X. Tian, L. Shan, S. Zhu, X. Xu, M. Jiang, L. Wang, D. Hui, Y. Wang, J. Lu and J. Gou, *Nanoscale*, 2014, 6, 8140-8148.
43. X. Liu, G. Zhou, S. W. Or and Y. Sun, *RSC Adv.*, 2014, 4, 51389-51394.
44. Z. Wang, H. Bi, P. Wang, M. Wang, Z. Liu, L. shen and X. Liu, *Phys. Chem. Chem. Phys.*, 2015, 17, 3796-3801.
45. W. Li, T. Qiu, L. Wang, S. Ren, J. Zhang, L. He and X. Li, *ACS Appl. Mater. Interfaces*, 2013, 5, 883-891.
46. P. Xu, X. Han, C. Wang, D. Zhou, Z. Lv, A. Wen, X. Wang and B. Zhang, *J. Phys. Chem. B*, 2008, 112, 10443-10448.
47. Z. Zhu, X. Sun, H. Xue, H. Guo, X. Fan, X. Pan and J. He, *J. Mater. Chem. C*, 2014, 2, 6582-6591.
48. H. Lv, X. Liang, Y. Cheng, H. Zhang, D. Tang, B. Zhang, G. Ji and Y. Du, *ACS Appl. Mater. Interfaces*, 2015, 7, 4744-4750.
49. H. Lv, G. Ji, X. Liang, H. Zhang and Y. Du, *J. Mater. Chem. C*, 2015, 3, 5056-5064.
50. G. Li, L. Wang, W. Li, R. Ding and Y. Xu, *Phys. Chem. Chem. Phys.*, 2014, 16, 12385-12392.
51. X. Li, J. Feng, Y. Du, J. Bai, H. Fan, H. Zhang, Y. Peng and F. Li, *J. Mater. Chem. A*, 2015, 3, 5535-5546.
52. J. Jiang, D. Li, S. Li, Z. Wang, Y. Wang, J. He, W. Liu and Z. D. Zhang, *RSC Adv.*, 2015, 19, 14584-14591.
53. H.-J. Yang, W.-Q. Cao, D.-Q. Zhang, T.-J. Su, H.-L. Shi, W.-Z. Wang, J. Yuan and M.-S. Cao, *ACS Appl. Mater. Interfaces*, 2015, 7, 7073-7077.
54. M. Han, X. Yin, L. Kong, M. Li, W. Duan, L. Zhang and L. Cheng, *J. Mater. Chem. A*, 2014, 2, 16403-16409.
55. S. Wen, Y. Liu, X. Zhao, J. Cheng and H. Li, *J. Magn. Magn. Mater.*, 2014, 354, 7-11.
56. B. Zhao, G. Shao, B. Fan, W. Zhao, Y. Xie and R. Zhang, *J. Mater. Chem. A*, 2015, 3, 10345-10352.
57. Q. Wang, Z. Lei, Y. Chen, Q. Ouyang, P. Gao, L. Qi, C. Zhu and J. Zhang, *J. Mater. Chem. A*, 2013, 1, 11795-11801.